


Tuning the magnetic anisotropy energy of atomic wires

Martin W. Prestel¹, Markus F. Ritter^{1,*}, Angelo Di Bernardo^{1,2}, Torsten Pietsch^{1,†} and Elke Scheer^{1,‡}

¹Universität Konstanz, Fachbereich Physik, Universitätsstraße 10, 78457 Konstanz, Germany

²University of Cambridge, Department of Materials Science and Metallurgy, 27 Charles Babbage Road, Cambridge CB3 0FS, United Kingdom

 (Received 2 October 2019; revised manuscript received 12 November 2019; published 30 December 2019)

In this article we present the fabrication of freestanding thin-film nanobridges of Ir. We perform magnetoconductance (MC) measurements of atomic contacts and monoatomic chains of Ir, realized by the mechanically controlled break-junction method. We observe continuous changes of the MC on the field scale of several tesla, as observed earlier for atomic-size contacts of two other strong paramagnets, Pd and Pt. The amplitude and the shape of the MC depend on the orientation of the magnetic field as well as on subtle details of the atomic arrangement, as confirmed by stretching studies of the contacts. Both positive dominant MC and negative dominant MC occur and are attributed to collinear or noncollinear alignment of the magnetic moments of the electrodes, respectively. By careful manipulation of the chain geometry we are able to study the transition between these two cases, which is hallmarked by a complex MC behavior. For special arrangements the MC almost vanishes. Our findings are in agreement with recent calculations of the geometry dependence of the magnetic anisotropy energy and open a route to tailor the MC behavior as required for particular applications.

DOI: [10.1103/PhysRevB.100.214439](https://doi.org/10.1103/PhysRevB.100.214439)

I. INTRODUCTION

Nonvolatile data storage has been performed using magnetic memory devices for many years. Further downsizing of storage units is limited by the superparamagnetic limit of traditional magnetic recording media. To overcome this limit while preserving the concept of magnetic encoding, the interest in magnetoelectronic properties of atomic-size structures [1] has strongly increased. While initially studies focused on atomic-size structures of the band ferromagnets Fe, Co, and Ni [2–4], it has been understood more recently that atomic-size structures of the strong paramagnets Ir, Pd, and Pt are well suited to study the emergence of magnetic order at the atomic scale [5–7]. For these systems which are close to the Stoner criterion of ferromagnetism in bulk systems [8], theoretical simulations show a magnetic ordering, if the size of the sample is reduced to the atomic scale [5–7,9–11]. For two of these metals, Pt and Pd, experimental evidence for local magnetic ordering has been found in small clusters, consisting of few atoms [12–14] and in atomic contacts, identified by magnetoconductance (MC) and anisotropic magnetoconductance measurements in Refs. [15,16]. There is ample theoretical evidence for Ir to exhibit a similar behavior [5,7,17,18]. The calculations show for three-atom-long idealized Ir chains between pyramidal electrodes that the magnetic anisotropy energy (MAE) of the apex atoms bridging the electrodes and the chain atoms may undergo a sign change upon subtle

variation of the configuration of the atomic chains [5]. This sign change in the MAE causes a transition from a collinear ground state of the magnetic moments inside the atomic chain, i.e., all moments pointing along the direction of the chain, to a noncollinear ground state, where the magnetic moment of one of the apex atoms points perpendicular to the chain. By generalizing this observation to atomic-size Ir chains with variable length and including disorder, we obtain our model shown in Fig. 1 which represents the central paradigm for the present work. The model assigns MC of the opposite sign to the two opposing ground states, as observed in Pt and Pd chains [15,16]. The transition between the two states has not been observed experimentally yet. As we show, in Ir these intermediate states can be resolved in MC curves showing strong variation on moderate field scales, a property which makes Ir atomic chains most suitable as magnetically controllable, ultimately miniaturized conducting devices.

II. EXPERIMENTAL METHODS

A. Sample fabrication and setup

We employ the mechanically controlled break-junction technique [19] to investigate atomic contacts of Ir by stretching free-standing Ir bridges. The bridges are fabricated by depositing a thin film (thickness of 80 nm) of Ir onto an insulating layer of Durimide [20] on top of a phosphor bronze or Kapton [21] substrate. The Ir thin films are grown by direct current (DC) magnetron sputtering in a high-vacuum chamber with a base pressure in the order of 10^{-8} Pa as confirmed by an *in situ* residual gas analyzer. To obtain an Ir metallic thin film that is fully relaxed on the Durimide/Kapton or Durimide/bronze substrate, we introduce 3.5 Pa of Ar into the chamber during growth and use a DC power of

*Present address: IBM Research - Zurich, Säumerstrasse 4, 8803 Rüschlikon, Switzerland.

†Present address: Carl Zeiss AG, Carl-Zeiss-Straße 22, 73447 Oberkochen, Germany.

‡elke.scheer@uni-konstanz.de

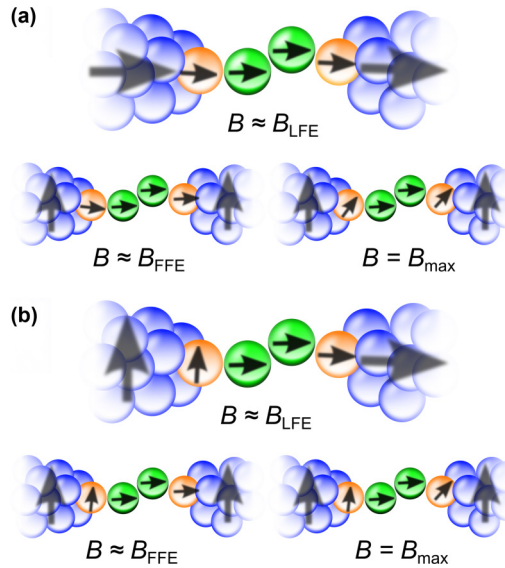


FIG. 1. Possible configurations of magnetic moments inside the contact region for generic traces. The apex atoms are highlighted in orange, the chain atoms in green, and the leads in blue. One possible configuration for negative MC curves is shown in panel (a) and for positive MC curves in panel (b). The labels B_{LFE} , B_{FFE} , and B_{max} refer to the magnetic field at which the extremes at low (finite) magnetic field amplitude B_{LFE} (B_{FFE}) occur and to the maximum applied field amplitude (B_{max}).

20 W, corresponding to an Ir deposition rate of approximately 0.038 nm/s. High-angle x-ray diffraction analysis and energy dispersive x-ray spectroscopy confirm that the Ir thin films are free from impurity phases. Details of the analyses are outlined in Appendix B. The as-grown Ir thin films are then structured via a subtractive patterning process as previously described by Strigl *et al.* [15]. In the pristine and unbroken state the bridges feature a typical conductance of $200 G_0$, where $G_0 = \frac{2e^2}{h}$ is the (spin-degenerate) conductance quantum with e being the elementary charge and h being Planck's constant. Each sample is cooled down to liquid helium temperature in a cryogenic vacuum where an electromigration process is employed to remove surface contamination and impurities (from the structuring process) and to reduce the number of structural defects in the constriction [15]. In this article we report data recorded from six samples.

B. Electronic transport measurements

The sample conductance is measured by applying a DC bias voltage to the sample and a reference resistor which is connected in series. The latter has a resistance of $R_{ref} = 103.5 k\Omega$ at 4 K. Differential conductance (dI/dV) spectra are recorded using the standard lock-in technique. The MC is investigated in fields applied perpendicular to the sample plane (z direction) of up to $B_z = \pm 8$ T. We define the magnetoconductance ratio (MCR) as the relative change in conductance upon applying a magnetic field:

$$\text{MCR} = \frac{G(B) - G_{\text{ext}}(B_{LFE})}{G_{\text{ext}}(B_{LFE})} \times 100\%, \quad (1)$$

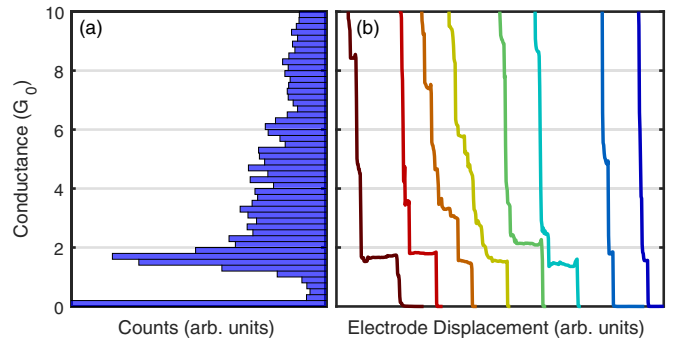


FIG. 2. (a) Typical conductance histogram of an Ir break-junction sample, calculated from 246 opening traces. (b) Exemplary opening traces with characteristic conductance plateaus.

where $G_{\text{ext}}(B_{LFE})$ is the conductance at the low-field extreme (LFE). We compare the amplitudes of the MC via their maximal deviation from $G_{\text{ext}}(B_{LFE})$. We call this maximal relative deviation MCR_{max} . The maximal absolute conductance change is denoted as ΔG and is indicated in units of the spin-polarized conductance quantum e^2/h .

III. RESULTS AND DISCUSSION

We first record the large-scale stretching dependence of the bridges for each sample by bending and relaxing the substrate repeatedly and computing conductance histograms from the opening traces. Figure 2(a) shows a typical conductance histogram that is composed of 246 opening traces and exhibits a distinct peak at $1.8 G_0$. Typical opening traces are presented in Fig. 2(b). They feature conductance plateaus just before breaking which we assign to a single-atom contact configuration. The measurements were performed with a voltage bias across the bridge of approximately 6 mV. For lower voltages the height of the peak in the conductance histogram corresponding to the last conductance plateau decreases. This effect can be attributed to pronounced zero-bias anomalies that were observed throughout all samples. These zero-bias anomalies will be discussed in a subsequent article. All samples exhibit a peak in the histograms at $1.8 G_0$. This finding is in accordance with experiments presented by Segers [22] who assigned this peak to the single-atom contact configurations of Ir.

A. Magnetoconductance behavior

We investigate the influence of a magnetic field applied perpendicular to the sample plane onto the conductance. A collection of MC traces is presented in Fig. 3. Red traces correspond to measurements performed while the magnetic field was increased, and blue traces correspond to a decreasing field (see also arrows in Fig. 3).

The MC traces that are highlighted in Fig. 3 by the shaded background are categorized as generic traces. These account for more than half of all measured MC characteristics; i.e., they represent the most common type of MC behavior found in the junctions investigated in this work. There are two types of generic MC traces. The traces may either feature a decrease in conductance with respect to the $G(B_{LFE})$ (negative MC)

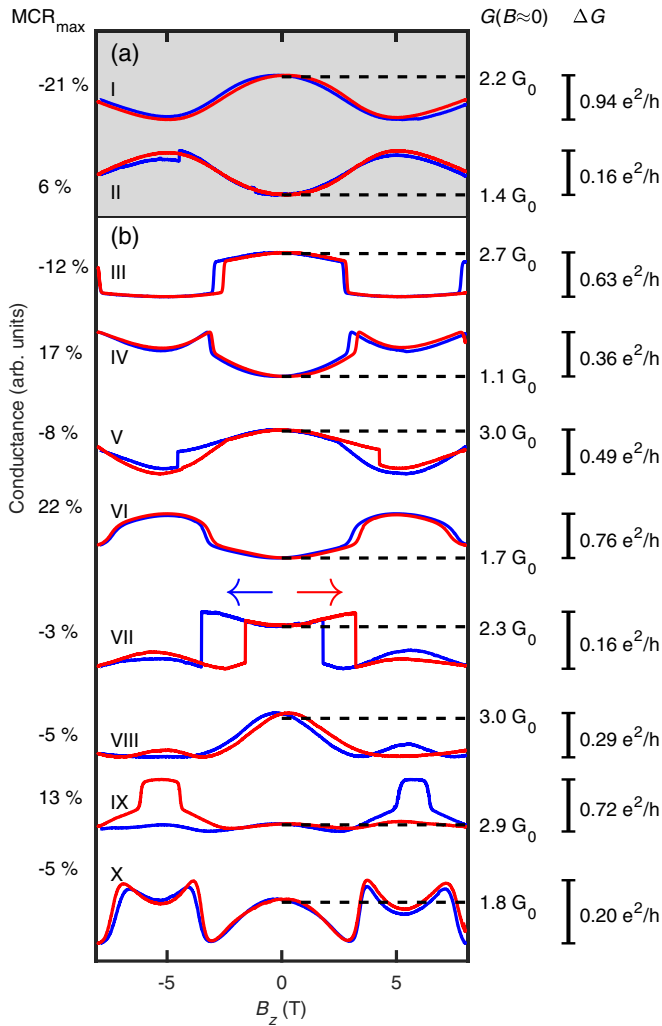


FIG. 3. Selected normalized MC traces of Ir contacts for different conductance values. The arrows indicate the sweep direction of the magnetic field. A magnetic field of up to ± 8 T was applied perpendicular to the sample plane. The MCR_{\max} values are indicated on the left-hand side. On the right-hand side the conductance at the LFE and the ΔG values in units of e^2/h are indicated.

or a conductance increase, once a magnetic field is applied (positive MC). These types of generic MC traces were discussed in detail by Strigl *et al.* [15,16] for atomic junctions of Pt and Pd. Within a minimal phenomenological model the authors assigned magnetic moments to the apex atoms and the chain atoms and a magnetic polarization to the leads. Considering the relative alignment of these moments or polarizations allows us to explain the behavior of the generic traces, as illustrated in Fig. 1. The model is based on two assumptions. First, a misalignment among the lead polarizations, the apex atoms' moments, or the chain atoms' moments reduces the conductance. Second, the lead polarizations can freely rotate while the moments of apex and chain atoms require stronger magnetic fields to change their orientation. The latter assumption is justified by the much larger MAE of the chain and apex atoms [5]. Hence, within this model, negative MC can be described by a collinear ground state of magnetic moments [Fig. 1(a)], whereas a noncollinear alignment accounts for

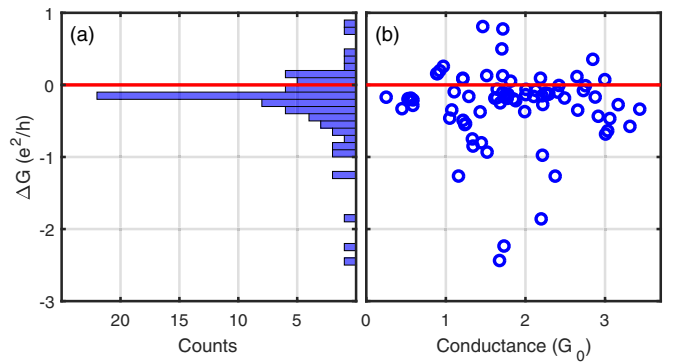


FIG. 4. (a) Histogram of maximal relative conductance change (ΔG) of all generic MC traces. (b) Distribution of ΔG with respect to the LFE conductance for all generic MC traces. The highest values for $|\Delta G|$ are found below $2.4 G_0$, where the atomic contact regime begins.

a positive MC [Fig. 1(b)]. In both cases, the conductance change is a result of a gradual out-of-plane rotation of the lead magnetic polarizations as the perpendicular field is increased. Finite field extremes (FFE) are located symmetrically at $B_{\text{ext}}^{\text{r}} = \pm 5.2$ T and correspond to an alignment of the lead magnetizations perpendicular to the current direction as their magnetic anisotropy energy (MAE) is overcome.

Another indication for magnetic ordering at the atomic scale is a hysteretic behavior at the LFE. The hysteresis (2Δ) can be analyzed by parabolic fits to the LFE for both sweep directions separately. The relative shift in LFE position yields hysteresis values 2Δ in the range of 0 to 0.55 T.

We compare the relative conductance variation of 77 generic MC traces by plotting the distribution of the conductance changes in Fig. 4(a) in units of the spin-polarized conductance quantum e^2/h . ΔG ranges from -2.5 to $+1 e^2/h$ ($-73\% < MCR_{\max} < +24\%$), hence the largest conductance changes are associated with a collinear magnetic ground state. The distribution of ΔG as a function of conductance is presented in Fig. 4(b). It shows a pronounced maximum around $-0.1 e^2/h$, i.e., a modulation that corresponds to a tenth of the contribution of a spin-polarized conductance channel. For conductance exceeding $2.4 G_0$ or being lower than $1 G_0$, $|\Delta G|$ decreases markedly. This result is in line with the hypothesis that only in small contacts, consisting of one or two atoms, does a local magnetic order form, as was theoretically predicted in Refs. [5,6]. Conductance values below the atomic contact regime are sparse since they correspond to disordered atomic contacts or near-tunneling contacts which are usually less stable. The few contacts investigated here reveal small $|\Delta G|$. These low values are in agreement with small local magnetic moments as expected for disordered contacts with varying bond lengths [5].

For a few contacts with a conductance at the LFE in the range from 1.8 to $2.4 G_0$, $|\Delta G|$ values exceed an amplitude of $1 e^2/h$. As discussed in Ref. [15], magnetostriction can be excluded as a possible origin because of the low magnetostrictive coefficients of paramagnets ($\Delta L/L = 2.4 \times 10^{-18} \text{ Oe}^{-2}$ for Ir [23]), the nonmonotonous and smooth field dependence of the conductance and the fact that the largest $|\Delta G|$ value

occurs for single-atom contacts and not for tunnel contacts. The large $|\Delta G|$ observed for some contacts indicates that more than one spin channel is affected by the reorientation. This is possible for Ir contacts because the conductance is larger than $1 G_0$ and thus must be formed by more than one channel. We are not aware of detailed transmission calculations of Ir atomic contacts or chains. However, it can be expected that, similar to Pt and Pd, at least three channels formed by hybridization of s and d orbitals carry the current [24,25]. More information about the channel content and their possible spin polarization can be obtained from shot noise measurements [26,27] and their statistical analysis along the lines of Ref. [28].

Among the generic traces the occurrence of negative ΔG is about 4 times higher than that of positive ΔG . In comparison, for Pt a factor of 2 and for Pd a factor of 5 higher abundance of negative ΔG have been observed [15,16]. In the framework of the microscopic model from Ref. [15] this finding implies a ground state that features a collinear alignment of magnetic moments. Since spin-orbit coupling (SOC) promotes the formation of a noncollinear ground state, these results are compatible with the trend of the SOC energies 1.09 eV (Pt), 0.94 eV (Ir), and 0.34 eV (Pd) of these transition metals [29].

The comparison of the FFE (B_{ext}) and the hysteresis 2Δ between Ir, Pd, and Pt further supports the conclusion that SOC plays a crucial role in the emergence of magnetism and the size of the magnetic moments in atomic contacts of strong paramagnets. A more detailed comparison of the three metals is made in Appendix A.

In addition to the generic traces, which can be explained by the aforementioned minimal collinear and noncollinear model, we observe various other shapes of MC traces. A selection is displayed in Fig. 3(b). These traces have a richer functional dependence, but share the features of a LFE, a FFE, and hysteresis. At variance with the generic traces, they may have a sweep-direction-dependent behavior (see curves III, V, and VII–IX) or very rapid changes with the magnetic field (see curves III, V, and VII). These features can be qualitatively described by a more refined model as sketched in the supplementary information of Ref. [15]. To this end one has to consider stretched bonds and different pinning strengths of the individual constituents of the junction. However, complex shapes like trace X are not fully understood within this model. This particular trace has been recorded within a stretching experiment, which is discussed in the next subsection.

B. Stretching dependence of MC curves

Thiess *et al.* [5] computed the magnitude of the magnetic moments of chain and apex atoms and their magnetic anisotropy energies (MAEs) as a function of the interatomic distance between the Ir atoms in a trimer configuration, i.e., a structure made of two apex atoms and a center atom between two leads. The MAEs of the apex atoms undergo a sign change at an elongation of 1 a.u. with respect to the equilibrium distance. For comparison, the interatomic distance in an atomic Ir chain amounts to about 4.2 to 4.5 a.u. (2.2 to 2.3 Å) [6,30]. For positive (negative) MAEs a collinear (noncollinear) alignment is energetically favorable. Therefore, the whole chain may

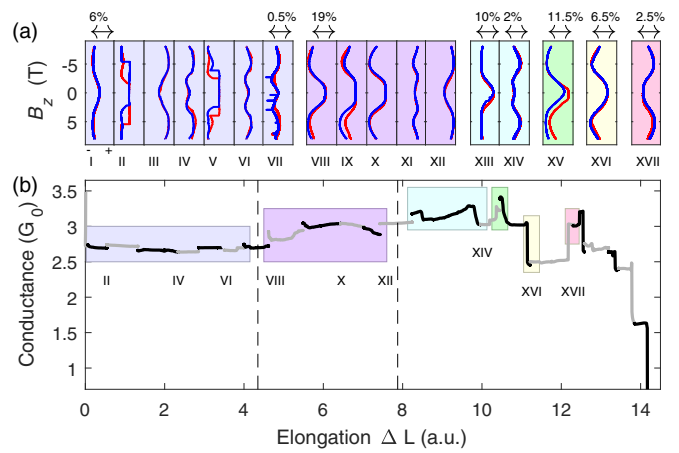


FIG. 5. Evolution of the MC when stretching an Ir chain. The initial state was prepared at $2.7 G_0$. Between the MC measurements, the chain was stretched, initially by about 0.6 a.u. per step and at larger steps distance towards the end of the experiment. Points at which a MC was recorded are indicated by a change in trace color. Conductance plateaus without rearrangements are shaded in the same background color. (a) MC traces as a function of the elongation ΔL . On the horizontal axis the MCR is plotted for better visibility of the MC change within one contact configuration. Arrows indicate the scaling of the axes. (b) Stretching curve of an Ir chain. The overall elongation before rupture corresponds to about 3.25 Ir bond lengths.

undergo a transition from a collinear to a noncollinear ground state upon stretching.

To investigate this transition, we stretch the break junction to a single-atom contact and perform a magnetic sweep. After this sweep we stretch the contact for about 0.5 a.u. while measuring its conductance. After each stretching step we record another MC trace. This procedure is repeated as long as the chain remains intact, i.e., the conductance stays above $1 G_0$. One typical trace of such an experiment is shown in Fig. 5(b). The individual conductance vs elongation traces are marked alternating in gray or black; sections with similar conductance and no sudden jumps are highlighted with colored boxes. For each box the corresponding MC traces are shown in Fig. 5(a). We interpret the jumps between the individual stable plateaus as atomic rearrangements which result in distinctly different and relaxed atomic configurations, in which the interatomic distance is close to its equilibrium. This assumption is supported by the fact that the first MC measurement after a jump shows the signature of a collinear ground state, i.e., negative MCR (with the exception of the last box, trace XVII, which was recorded not immediately after a jump but after a further stretching of about 0.1 a.u.). While stretching a given configuration, i.e., within a colored box, the MC traces undergo a transition from that initial collinear ground state into a noncollinear ground state. This transition is particularly evident for traces VIII to XII. The elongation ΔL between these MC traces is 0.87, 0.95, 0.58, and 0.41 a.u., respectively. Between traces VIII and X, no significant change is observed, as is expected from the calculations by Thiess *et al.* [5] for small stretching. Nevertheless, traces IX and X start to flatten out around zero field as the contact is elongated. This indicates the onset of a change of

the ground state alignment. In Ref. [5], a pronounced change of the MAE as a function of the bond length including a sign change from negative to positive MAE of the apex atoms is predicted. After the fourth stretching within that box, trace XI is recorded. It exhibits additional extremes at about 2.5 T. It is not possible to explain this curve with the minimal model described above. A minimal model that qualitatively explains this curve with five extremes requires that the MAE of the apex atoms and the electrodes is different for the left and right part of the chain. To qualitatively understand the observation, we conclude that the MAE of at least one apex atom and its electrode is close to a sign change from collinear to noncollinear magnetization. Since the MAE of this apex atom is small compared to the MAE of chain atoms, its magnetic moment starts rotating at low field, which leads to a conductance increase. Consequently the conductance extremes around ± 2.5 T might then correspond to a fully perpendicular aligned moment with a small MAE. After an additional stretching step, the MAE of one apex atom becomes positive, resulting in the shape of a noncollinear ground state, i.e., positive MCR (trace XII). At the end of the purple box, the total elongation of the chain is about 2 Å (corresponding to about 4 a.u.). This value is close to the bonding length of an Ir atom in a monoatomic wire [6,30]. Hence, we assume that the atomic arrangement becomes unstable, which leads to a reconfiguration of the contact just after trace XII.

IV. SUMMARY AND CONCLUSION

In this article we present a fabrication scheme for nanoscale free-standing bridges of Ir, fabricated by sputtering, electron beam lithography, and reactive ion etching. With these nanobridges we arrange atomic contacts and monoatomic chains and measure their magnetotransport properties at low temperature. We observe strong variations of the conductance as a function of perpendicular magnetic field with a variety of functional shapes. The majority of the curves can be qualitatively explained using a model which was developed for atomic-size structures of Pt and successfully applied for contacts of Pd, however, with quantitatively different amplitudes and field strengths. The observed material dependence is in good agreement with expectations based on calculations of atomic contacts as well as from bulk properties. The results of these studies compared with literature simulations on atomic chains provide the evidence that the atomic magnetic moments in the atomic chains may be ordered and that a collinear alignment of the electrodes' polarizations is adopted preferentially for relaxed chains. When stretching the chains, we observe distinct changes in the MC response, which can be understood as a gradual transition to the noncollinear ground state of the magnetic moments. The maximum elongations before contact instability are comparable with theoretical calculations for an Ir trimer. We are able to stabilize contacts at the transition point where the MC reveals a more complex behavior beyond our phenomenological model. These transition states between collinear and noncollinear configurations have been observed in several stretching experiments and indicate that the local

magnetic arrangement in such contacts results from a subtle interplay between several parameters, such as bond length and MAE varying from site to site. Vice versa, this finding implies that the local magnetic order on the subatomic scale can be tuned mechanically.

ACKNOWLEDGMENTS

We thank M. Hagner, S. Haus, S. Andreev, and J. W. A. Robinson for help in the sample preparation and magnetic characterization. We thank A. Smogunov and S. Heinze for helpful discussion. M.W.P. acknowledges financial support from the Carl Zeiss Foundation and M.W.P., A.D.B., and E.S. acknowledge financial support from the Leverhulme Trust through an International Network Grant (Grant No. IN-2013-033).

APPENDIX A: COMPARISON WITH PD AND PT

To compare our findings in Ir with Pt and Pd, the first quantity we consider is the maximum effect size, i.e., the MCR_{max} value. $|\text{MCR}_{\text{max}}| > 20\%$ are observed in a conductance range from 0.26 to 2.4 G_0 for both polarities, i.e., for collinear as well as for noncollinear ground states, though, with a strong favor for the collinear ground state. Strigl *et al.* [15] found MCR_{max} to range from -40% to 40% for Pt. The magnetic moments of atoms in monoatomic chains have been calculated in the literature [11,17,31], yielding higher magnetic moments for Ir than for Pt. Since this result implies a higher spontaneous spin-splitting in the local density of states of Ir and the application of a magnetic field changes the overlap of wave functions between adjacent atoms, one expects a larger $|\text{MCR}_{\text{max}}|$ for Ir than for Pt. However, for realistic contact geometries the situation is more complicated. The magnetic moment per atom μ in chains of Ir and Pt crucially depends on the interatomic bond lengths [5,6]. Consequently, the magnetic moment per atom μ^{Pt} might be larger than μ^{Ir} for certain bond lengths, and it remains challenging to draw general conclusions from the comparison of both transition metals.

Besides the amplitude of the MC, the magnetic field B_{ext} at the FFE is expected to correlate with μ as well. The distribution of $|B_{\text{ext}}^{\text{Ir}}|$ is centered at 5.2 T, ranging from 4.7 to 6.5 T in the case of Ir. For Pd, $|B_{\text{ext}}^{\text{Pd}}|$ is located at lower fields between 3 and 5 T [16], while for Pt $|B_{\text{ext}}^{\text{Pt}}|$ ranges between 4 and 7 T [15]. Strigl *et al.* [16] argue that $\mu^{\text{Pd}} > \mu^{\text{Pt}}$ implies a higher Zeeman energy for Pd which relates to a stronger torsional force on the localized magnetic moments, resulting in $|B_{\text{ext}}^{\text{Pd}}| < |B_{\text{ext}}^{\text{Pt}}|$. At equilibrium bond length, the spin magnetic moments of Pd and Ir are similar. For both metals the magnetic moments increase upon elongation of the interatomic bonds. Eventually, both the spin moment and the orbital moment of Ir exceeds the respective moments of Pd [31]. Following this reasoning the measured distribution of $|B_{\text{ext}}^{\text{Ir}}|$ is not consistent with theory. Nevertheless, one might speculate that the higher SOC of Ir compared to Pd stabilizes the magnetic order in Ir, causing $|B_{\text{ext}}^{\text{Ir}}| > |B_{\text{ext}}^{\text{Pd}}|$.

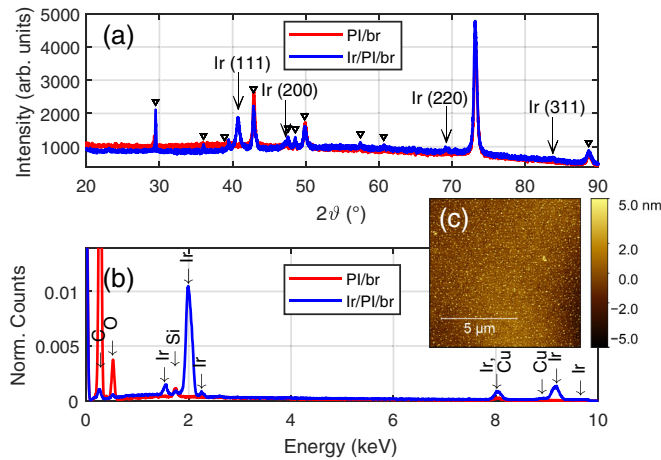


FIG. 6. (a) High-angle x-ray diffraction traces of the substrate [polyimide on bronze (PI/br)] and the Ir film on this substrate (Ir/PI/br). The additional peaks in the Ir/PI/br trace only originate from Ir; peaks which also appear for the substrate are marked with a triangle. (b) Traces of the energy dispersive x-ray spectroscopy for the substrate and the Ir film. Additional peaks for the Ir film trace coincide with energies expected for Ir. (c) AFM image of the sputtered Ir film on the PI. The rms roughness of this film is $R_q = 2.2$ nm.

This assumption is supported by a comparison of the hysteretic behavior that is a measure for the MAE in the contact geometry. By applying a parabolic fit to the LFE of the generic MC traces we extract hysteresis shifts 2Δ in the field sweep direction ranging from 0 to 0.55 T. In Pt and Pd, the hysteresis was found to range from 0 to 0.8 T and from 0.14 to 0.31 T, respectively [15,16]. These results indicate that the MAE indeed correlates with SOC as reported earlier for metal clusters of these transition metals [32].

APPENDIX B: ANALYSIS OF THE IR FILM

The sputtered Ir films were checked after the deposition by different means. To ensure the quality and exclude defects, the films were examined by optical, scanning electron, and atomic force microscopy. One example of an atomic force microscopy (AFM) image is displayed in Fig. 6(c). The rms roughness for $10 \times 10 \mu\text{m}^2$ of the film is calculated to be $R_q = 2.2$ nm. In addition to the surface inspection, we also analyzed the films by high-angle x-ray diffraction as well as by energy dispersive x-ray spectroscopy. Both measurements were done on the bare substrate as well as on the sputtered film to identify the background signal originating from the substrate. The results of both experiments are shown in Fig. 6 and confirm the purity of the Ir film.

- [1] N. Agraït, A. L. Yeyati, and J. M. van Ruitenbeek, *Phys. Rep.* **377**, 81 (2003).
- [2] M. Viret, M. Gabureac, F. Ott, C. Fermon, C. Barreateau, and R. Guirado-Lopez, *Eur. Phys. J. B* **51**, 1 (2006).
- [3] M. R. Calvo, J. Fernández-Rossier, J. J. Palacios, D. Jacob, D. Natelson, and C. Untiedt, *Nature (London)* **458**, 1150 (2009).
- [4] S. Egle, C. Bacca, H.-F. Pernau, M. Huefner, D. Hinzke, U. Nowak, and E. Scheer, *Phys. Rev. B* **81**, 134402 (2010).
- [5] A. Thiess, Y. Mokrousov, and S. Heinze, *Phys. Rev. B* **81**, 054433 (2010).
- [6] A. Delin and E. Tosatti, *Phys. Rev. B* **68**, 144434 (2003).
- [7] V. M. García-Suárez, D. Z. Manrique, C. J. Lambert, and J. Ferrer, *Phys. Rev. B* **79**, 060408(R) (2009).
- [8] E. C. Stoner, *Proc. R. Soc. A* **165**, 372 (1938).
- [9] A. Bergman, J. Hellsvik, P. F. Bessarab, and A. Delin, *Sci. Rep.* **6**, 36872 (2016).
- [10] C. Heiliger, P. Zahn, and I. Mertig, *Mater. Today (Oxford, U.K.)* **9**, 46 (2006).
- [11] A. Smogunov, A. Dal Corso, and E. Tosatti, *Phys. Rev. B* **78**, 014423 (2008).
- [12] B. Sampedro, P. Crespo, A. Hernando, R. Litrán, J. C. Sánchez López, C. López Cartes, A. Fernandez, J. Ramírez, J. González Calbet, and M. Vallet, *Phys. Rev. Lett.* **91**, 237203 (2003).
- [13] B. V. Reddy, S. N. Khanna, and B. I. Dunlap, *Phys. Rev. Lett.* **70**, 3323 (1993).
- [14] J. A. Alonso, *Chem. Rev.* **100**, 637 (2000).
- [15] F. Strigl, C. Espy, M. Bückle, E. Scheer, and T. Pietsch, *Nat. Commun.* **6**, 6172 (2015).
- [16] F. Strigl, M. Keller, D. Weber, T. Pietsch, and E. Scheer, *Phys. Rev. B* **94**, 144431 (2016).
- [17] T. Nautiyal, T. H. Rho, and K. S. Kim, *Phys. Rev. B* **69**, 193404 (2004).
- [18] A. Thiess, Y. Mokrousov, S. Heinze, and S. Blügel, *Phys. Rev. Lett.* **103**, 217201 (2009).
- [19] Y. Kim, H. Song, F. Strigl, H.-F. Pernau, T. Lee, and E. Scheer, *Phys. Rev. Lett.* **106**, 196804 (2011).
- [20] Fujifilm Electronic Materials, Durimide 115A, 2019.
- [21] Fralock, Cirlex, 20 mil, 2017.
- [22] R. Segers, Quantum properties of nano-bridges in iridium, Dissertation, Universiteit Leiden, 2002.
- [23] E. Fawcett, *Phys. Rev. B* **2**, 3887 (1970).
- [24] J. Fernández-Rossier, D. Jacob, C. Untiedt, and J. J. Palacios, *Phys. Rev. B* **72**, 224418 (2005).
- [25] L. A. Zotti and R. Pérez, *Phys. Rev. B* **95**, 125438 (2017).
- [26] M. Kumar, O. Tal, R. H. M. Smit, A. Smogunov, E. Tosatti, and J. M. van Ruitenbeek, *Phys. Rev. B* **88**, 245431 (2013).
- [27] A. Burtzloff, A. Weismann, M. Brandbyge, and R. Berndt, *Phys. Rev. Lett.* **114**, 016602 (2015).
- [28] R. Vardimon, M. Klionsky, and O. Tal, *Phys. Rev. B* **88**, 161404(R) (2013).
- [29] O. K. P. W. Andersen, *Phys. Rev. B* **2**, 883 (1970).
- [30] R. H. M. Smit, C. Untiedt, G. Rubio-Bollinger, R. C. Segers, and J. M. van Ruitenbeek, *Phys. Rev. Lett.* **91**, 076805 (2003).
- [31] J. C. Tung and G. Y. Guo, *Phys. Rev. B* **81**, 094422 (2010).
- [32] L. Fernández-Seivane and J. Ferrer, *Phys. Rev. Lett.* **99**, 183401 (2007).